DYNAMIC STALL : THE CASE OF THE SCULLING TYPE MARINE PROPULSOR

M. A. Kotb

Department of Naval Architecture and Marine Engineering
Faculty of Engineering, Alexandria University, Alexandria, Egypt.
E-mail: Abbas@alex.eun.eg

ABSTRACT

A study of dynamic stall is presented to illustrate its effects on airfoil lift and drag coefficients so that these effects can be included in the hydrodynamic analysis of sculling type marine propulsor. A literature review for different tests used to explain the phenomenon of dynamic stall is presented. A semiempirical method was implemented in sculling propulsion loads and power analysis. The method was first applied to a typical airfoil whose stationary data over a wide range of incidence and Reynolds number was available. Dynamic lift and drag data were generated over a range of Reynolds numbers and pitch rate parameters. This data was used as input in a single pass multiple streamtube analysis of a sculling propulsion system. It was shown that loads, and power on the blades and hence efficiency may be underestimated, particularly at partloads if dynamic stall is not considered.

Keywords: Hydrodynamic Propulsion , Sculling Propellers, Dynamic Stall, Airfoils

NOMENCLATURE

A	blade total planform area (m^2)
b	blade semi stroke (m)
C	blade chord (m)
C_L	sectional lift coefficient
C_D	sectional drag coefficient
C_M	sectional moment coefficient
dK_S	elemental side force coefficient
dK_T	elemental thrust coefficient
dK_P	elemental power coefficient
F_y	side force
J	advance coefficient = V_A/V_{Tmax}
K_T	thrust coefficient = $T/\rho(V_{Tmax})^2 A$
K_S	side Force coefficient = $F_y/\rho(V_{Tmax})^2 A$
K_P	power coefficient = $P/\rho(V_{Tmax})^3 A$
N	number of blades
P	power (W)
Re	Reynolds number = $V_R c/\nu$
T	propeller thrust (N)
t	blade maximum thickness (m)
V_A	axial flow at the wing (m/s)
V_R	resultant velocity to the blade (m/s)
V_t	transverse wing speed (m/s)
V_{tmax}	maximum transverse speed(m/s)
x, y, z	coordinate system
α	angle of attack to the blade element (deg)
α_{DS}	dynamic stall angle (deg)
α_{ss}	static stall angle (deg)
α_m	modified angle of attack to blade element (deg)
α^*	reference angle of attack to blade element (deg)
β	flow angle relative to y axis (deg)
γ	gamma function ;empirical constant
η	propeller efficiency = (K_T/K_P) J
ν	water kinematic viscosity(m^2/s)
ρ	water density (kg/m^2)
θ	blade setting angle relative to y axis (deg)

INTRODUCTION

Sculling propulsion system consists of one or two wings, mounted vertically behind a ship, and which move sideways back and forth. The angles of incidence of the wings are adjusted so that a thrust force is delivered. Recently, interest has been renewed in this type of ship

propulsion. Experimental and theoretical work is currently underway to examine the performance capabilities and potentials of sculling propulsion system [1].

A sculling propeller blade element experiences changes in angle of attack, as it oscillates back and forth along its trajectory. As the blade oscillates, the transverse location changes and the airfoil experiences a variation of incidence pending on type of transverse motion, and extent and value of ship's wake. This variation of incidence is coupled to a variation of the relative flow speed. For high enough values of transverse speed, and/or low enough axial water velocity, the elements static stall value will be exceeded over portions of the blade path. The time rate of change of angle of attack, $\dot{\alpha}$ causes delays in both the onset of and the recovery from stall to values of a above and below, respectively. A hysteresis is added to the airfoil characteristics. This is termed dynamic stall and results in increasing both required system power output and peak hydrodynamic torque at a given ship speed. These effects significantly impact drive train/ engine sizing and system reliability.

The dynamic stall phenomenon is extremely complex. Factors influencing it are airfoil geometry, Reynolds number, reduced frequency, angle of attack (both mean value and amplitude). The problem of dynamic stall may be encountered in other engineering applications. Examples include wind energy converters [2] water turbines [3] helicopter rotors [4] and cycloidal marine propellers [5].

The dynamic stall phenomenon is described in this paper, both qualitatively and in the form of a semiempirical prediction method. Sample calculations are presented for a representative sculling propulsion case to show the effect of dynamic stall on loads, power, and hence efficiency.

DYNAMIC STALL PHENOMENON

Dynamic stall, as defined earlier, differs substantially from the familiar static stall encountered at constant or slowly varying angles of attack. If it occurs, it can produce a lift and nose down moment with peak values much greater than the corresponding static loads. Load variations of such high magnitudes may exceed structural static margins and may significantly reduce the fatigue life of the system. In addition, the system performance may deviate from predicted values, thereby affecting the matched performance of the propeller/gearbox/prime mover design. The effects of dynamic stall on lift and moment coefficients of a typical airfoil pitching at a rate of 8.2 rad/sec are shown in Figures 1-a and 1-b reproduced from Reference 2.

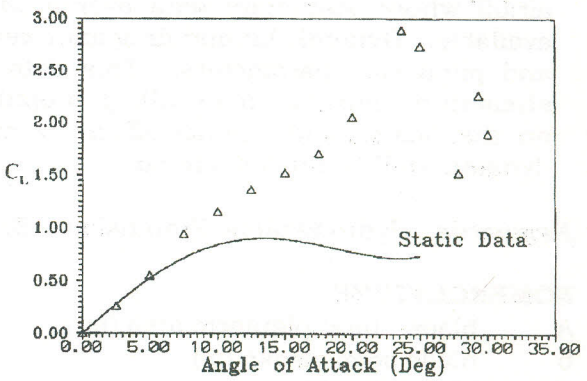

Figure 1-a Dynamic stall characteristics of NACA 0012 airfoil at $\dot{\alpha}$ =8.2 rad/s.(C_L data)[2]

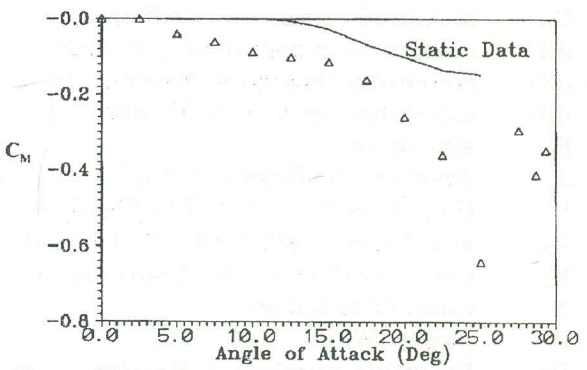

Figure 1-b Dynamic stall characteristics of NACA 0012 airfoil at $\dot{\alpha}$ =8.2 rad/s (C_M Data) [2]

Dynamic stall may be encountered by airfoils or lifting surfaces which are oscillating or subject to time varying incident flows. Dynamic stall is an unsteady phenomenon and its mechanism is complex and not completely understood. The primary

characteristics of dynamic stall are its occurrence an angle of attack greater than the stall angle, followed by the shedding of vorticity form the leading and trailing edges. When the airfoil oscillates about a mean angle of attack α, that exceeds the static stall angle, a separation bubble forms near the leading edge. The flow tends to reattach aft of the bubble and a second bubble occurs near the trailing edge.

As the angle of attack increases, the leading edge bubble grows in strength. The suction pressure at these bubbles or vortices increases. The leading edge vortex gains in strength and moves aft as the trailing edge suction pressure increases. The leading edge vortex breaks free of the surface and moves aft as it gains in strength. The increased suction pressure associated with the vortex also moves aft. Meanwhile, the aft vortex is swept off the trailing edge. The rearward movement of the vortices produces an increased vertical load on the airfoil and rearward shift of the center of pressure. This results in a significant increase in nose down pitching moment.

The dynamic stall process has been under investigation for the past two decades, and significant progress has been made towards understanding the physical processes associated with rapidly pitching an airfoil beyond its static stall angle of attack. The work of Carr [6] and Visbal [7] describe the physical process of dynamic stall.

Considerable work has been accomplished on the testing of various airfoils under either various pitch rates or oscillating conditions to determine the basic characteristics during dynamic stall. These tests and data have been used not only to define and understand the dynamic stall phenomenon but also to develop models to predict the loads associated with dynamic stall.

Several semiempirical methods have been developed based on experimental data. These methods are used for estimating the forces and moments on oscillating airfoils. The different methods were compared by McCroskey [8].

MODELING OF DYNAMIC STALL

The method used in this paper is that of References 9 and10. The hysteresis associated with dynamic stall is modeled in a manner which employs the two dimensional, stationary airfoil data. As an airfoil oscillates, points representing the lift and drag coefficients do not follow the static curves, but form hysteresis loops, (see Figure 2.)

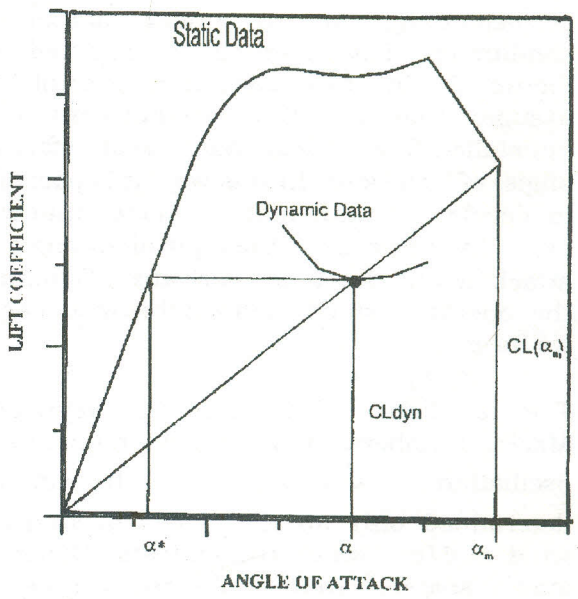

Figure 2 Dynamic stall model

If lift and drag variations versus angle of attack in the stationary condition are known, and if the angle of attack is α, then a modified angle of attack α_m is defined as:

$$\alpha_m = \alpha - \gamma\sqrt{\mathrm{Abs}\left(\frac{C\dot{\alpha}}{2V_R}\right)} \qquad \dot{\alpha} > 0 \qquad (1)$$

$$\alpha_m = \alpha + \frac{\gamma}{2}\sqrt{\mathrm{Abs}\left(\frac{C\dot{\alpha}}{2V_R}\right)} \qquad \dot{\alpha} > 0 \qquad (2)$$

where γ is a function determined empirically from wind tunnel measurements of oscillating airfoils, and $\dot{\alpha}$ is time change rate of angle of incidence. This relation is used as a bridge between static and

dynamic stall by defining the dynamic stall angle of attack as a function of the static angle of attack.

The instantaneous lift, drag, and moment coefficients (or dynamic coefficients) are given as

$$(C_L)_{dyn} = \text{Static } C_L(\alpha_m)\frac{\alpha}{\alpha_m} \quad (3)$$

$$(C_D)_{dyn} = \text{Static } C_D(\alpha_m) \quad (4)$$

$$(C_M)_{dyn} = \text{Static } C_M(\alpha_m) \quad (5)$$

where $C_L(\alpha_m)$, $C_D(\alpha_m)$, nd $_M(\alpha_m)$ are the lift, drag, and moment coefficients corresponding to α_m under stationary conditions. This method is depicted in Figure 2. In this case, it is possible to assume that real flow is equivalent to a nonstalled flow corresponding to an effective angle of attack α^*. In this way, it is possible to develop a mathematical model that will explicitly determine the equivalent angle of attack α and its time derivative. Denoting the operator which defines this model as f, we have

$$\alpha^* = f(\alpha, \dot{\alpha}) \quad (6)$$

The function f depends on Reynolds, Mach numbers, and reduced frequency of oscillation $\sqrt{C\dot{\alpha}/2V_R}$. It can be determined only on the basis of extensive wind and/or water tunnel tests. Dynamic stall angles were plotted versus a nondimensional pitch rate $\sqrt{C\dot{\alpha}/2V_R}$ and data were shown to exhibit a linear relation. The slope was defined as the proportionality constant γ.

$$\gamma = \frac{\Delta\alpha_{DS}}{\Delta\sqrt{C\dot{\alpha}/2V_R}} \quad (7)$$

The empirical factor γ is different for the lift and drag angle of attack calculations. It was found out, based on a large number of measurements on different types of airfoils that:

$$\gamma_L = 1.04 + 6.0*\left(\frac{t}{C}\right) \quad (8)$$

$$\gamma_D = 0.85 + 2.5*\left(\frac{t}{C}\right) \quad (9)$$

where (t/C) is the thickness to chord ratio of the airfoil. Typical examples of experimental correlation between static and dynamic performance of two different airfoil types are shown in Figure 3.

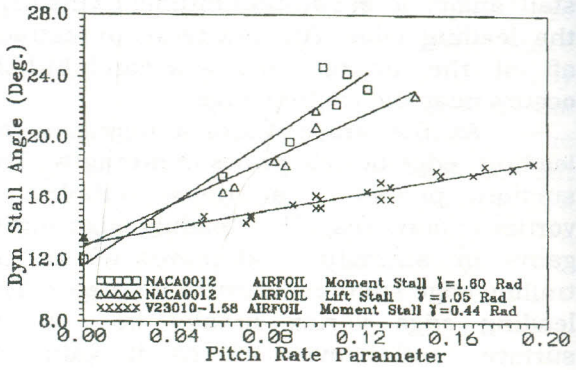

Figure 3 The constant γ for different airfoil sections

SCULLING PROPELLER: CASE STUDY

The sculling propulsion system, studied by the author [11], was used as a sample application to demonstrate the effects of dynamic stall on its hydrodynamic performance. Its basic characteristics are :

No of blades	1
Blade chord	1 m
Blade span	8 m
Speed of advance	8 m/s
Blade semi stroke ratio (b/c)	10
Blade profile	NACA 0021

The performance analysis was studied using a single pass multiple streamtube theory combined with blade element analysis. The analysis was modified to permit including dynamic effects into the calculations. Derivation details are given in Reference 11.

RESULTS AND DISCUSSION

It has been seen and verified through experimental data that dynamic effects alter the static airfoil section stall characteristics. A large amount of data exists in the literature for stationary airfoils tested in wind/water tunnels and the results are given in terms of lift, drag, and moment coefficients as functions of mainly angle of attack at possibly different

Reynolds and Mach numbers. These results are "stationary" in the sense that no time variation for incidence is included; see for example Reference 12.

In order to examine the effect of profile pitch rate on its aero/hydrodynamic data in a step to supplement the existing data with the necessary pitch rate effects, a typical airfoil section designated "NACA0021" was selected for this purpose. This particular airfoil section was selected as its documented data cover a full range of incidence (0 through 180 Degrees) and a reasonable range of Reynolds number (10^4 - $5x10^6$) [13]

The pitch rate $\dot{\alpha}$ is given in non dimensional pitch rate parameter as:

$$\text{Pitch Rate} = \sqrt{\frac{C\dot{\alpha}}{2V_R}} \qquad (10)$$

and for a constant Reynolds number, the pitch rate is:

$$\text{Pitch Rate} = \sqrt{\frac{C^2\dot{\alpha}}{2\nu Re}} \qquad (11)$$

Physical interpretation of $\sqrt{C\dot{\alpha}/2V_R}$ can be obtained by noting that C/V_R is approximately the time it takes for a particle of fluid to travel from the leading edge to the trailing edge of the airfoil and is therefore, a measure of the time it takes for stall to fully develop. Hence, the term $C\dot{\alpha}/V_R$ is the $\Delta\alpha$ that can occur before stall effects become significant. Experimental findings have shown that pitch rate has more effect on lift stall than on moment stall which causes high control loads. Furthermore, the beneficial effects of dynamic stall on retarding the stall are reduced at higher speeds.

The method explained earlier, (Equations 1 through 11) was used to generate a number of $C_L(\alpha)$ and $C_D(\alpha)$ at a number of constant Reynolds number and pitch rate parameters for the NACA0021 profile. The results are given for pitch rate values of -0.4 to 0.4 rad/s at 0.1 rad/s increment. Due to space limitations, sample results are given for one Reynolds number; namely Re= $5x10^6$. The results for dynamic lift and drag are shown in Figures 4-a and 4-b respectively. The static data corresponding to zero pitch rate (non oscillating airfoils) are shown on the same plot as a basis for comparisons. The plots show that for positive pitch rates, C_L increases while C_D decreases. The opposite is true for negative pitch rates. In other words, positive pitch rate has a favorite effects on both C_L and C_D while negative pitch rate will result in lower C_L and higher C_D values for the same Reynolds number.

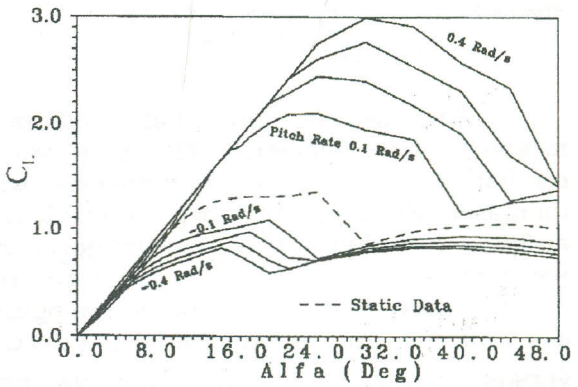

Figure 4-a Generated dynamic lift data for NACA0021 versus angle of incidence and pitch rate

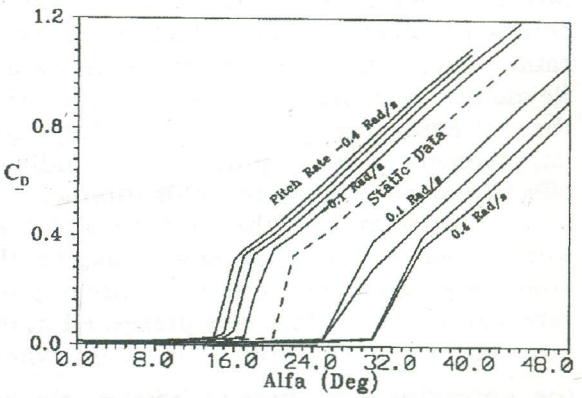

Figure 4-b Generated dynamic drag data for NACA0021 versus angle of incidence and pitch rate

The effect of dynamic stall is less significant for the region below static stall. This was quite clear for the case studied and shown in figures (4-a) and (4-b). These curves are useful in providing dynamic sectional data for applications involving oscillating airfoils.

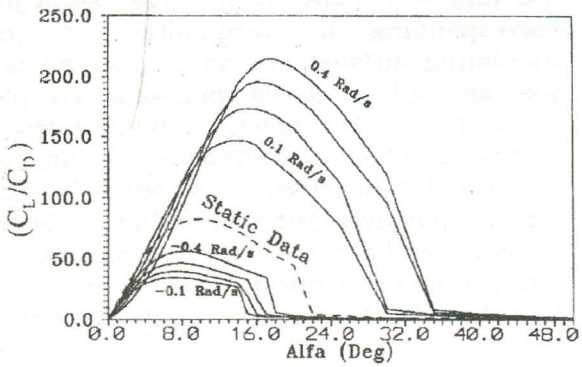

Figure 4-c Generated dynamic lift/drag ratio for NACA))21 versus angle of incidence and pitch rate

The section lift/drag ratio is a measure of its efficiency. This ratio for non oscillating airfoil data increases with increased Reynolds number. For oscillating airfoils, the pitch rate is another governing parameter on airfoil aero/hydrodynamic effectiveness. The results plotted in figures 4-a and 4-b are combined to yield (C_L/C_D) versus angle of attack and its time derivative. This is shown in Figure 4-c It is also noted that positive pitch rate has a favorable effect on the C_L/C_D ratio in contrast to negative rates which reduce that ratio. The trend is similar to increasing Reynolds number. It is noted here that there is equivalency between boundary layer improvement due to pitch rate induced effects and increasing Reynolds number.

Furthermore, the results obtained were used to examine how sensitive the stationary airfoil section data are to pitch rate variations. This was presented in the form of $C_{L\dot{\alpha}}$, $C_{D\dot{\alpha}}$ and $(C_L/C_D)\dot{\alpha}$ where the subscript $\dot{\alpha}$ here stands for the derivative with respect to $\dot{\alpha}$ i.e. $\delta/\delta_{??}$. The results are given in Figures 5-a, 5-b, and 5-c respectively. Maximum values for lift, and drag pitch rate derivatives are around the same incidence angle (about 25°). The lift/drag ratio pitch rate derivative takes place a little earlier (at about 16° incidence). These derivatives are useful in assessing the effects of unsteady pitch on the resulting aero/hydrodynamic airfoil data using "stationary" section data.

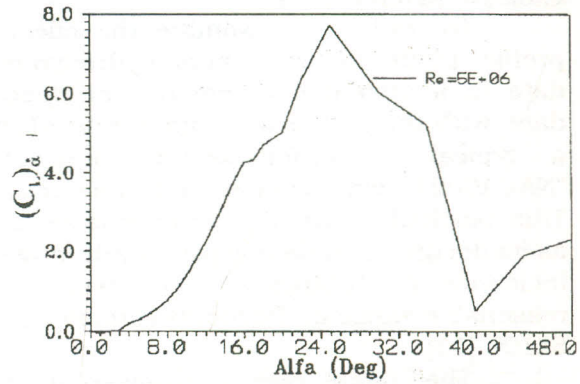

Figure 5-a Lift coefficient derivative with respect to pitch rate for NACA0021 at Re=5E+06

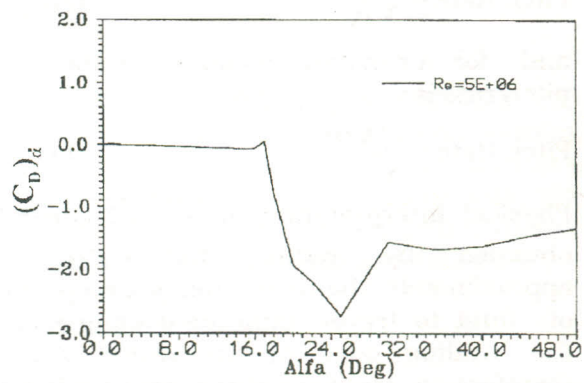

Figure 5-b Drag coefficient derivative with respect to pitch rate for NACA0021 at Re = 5E+06

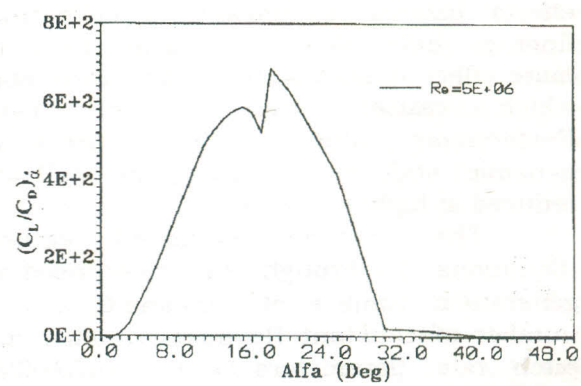

Figure 5-c Lift/drag Ratio derivative with respect to pitch rate for NACA0021at Re=5E+06

Analysis procedure outlined by the author [11] was modified as such to include dynamic effects. The modified model was applied to the case of sculling type

propulsor whose particulars are given above. The thrust generated, expressed in terms of thrust coefficient K_T, is plotted versus advance coefficient J in Figure 6 The results are given with and without dynamic stall. It is shown that dynamic stall effects are more pronounced at lower J values (part load conditions). For values of advance coefficients past the maximum K_T position, the response to dynamic stall is negligible. The reason can be attributed to the fact that K_T, is directly proportional to the quantity $(C_L \cos\beta - C_D \sin\beta)$ where β is the relative flow angle to the blade section. When J decreases, the angle of incidence α increases as seen from:

$$\alpha = \theta - \arctan\left(J / \sqrt{1-(y/b)^2}\right) \qquad (12)$$

where θ is the blade setting angle, y is its transverse location, and b is the blade semistroke. At some regions, α might exceed the stall angle. Consequently C_L increases and C_D decreases. So, this results in increased K_T. On the otherhand, operating at high J value means lower incidence (lower than the static stall angles; that is the linear region) and hence, dynamic effect is insignificant.

Side force coefficient, K_S, at a number of advance coefficient is shown in Figure 7. Dynamic stall also affects the resulting side force at J values below the one at which K_S is maximum. This is similar to the effect on thrust. However, the effect is not as much as that on the thrust. This can be explained on the ground that K_S is proportional to the quantity $(C_L \sin\beta + C_D \cos\beta)$ and for low J value, α is high and accordingly, C_L increases while C_D decreases so, K_S will be higher. The corresponding power K_P required by the propulsor with and without stall at different advance speeds is shown in Figure 8.

If the dynamic stall is not included in the analysis, the propulsion efficiency is not accurately predicted particularly at part loads; (see Figure 9). This conclusion is expected when the results obtained in Figures 6, 7, and 8 are examined. Since both K_T and K_P increase at different rates, the propulsive efficiency expressed as: $\eta=(K_T/K_P)J$ increases as well.

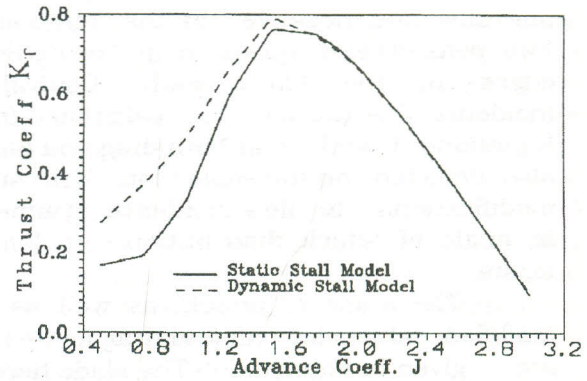

Figure 6 Sculling propulsor thrust variation versus advance coefficient with and without dynamic stall [θ=75°]

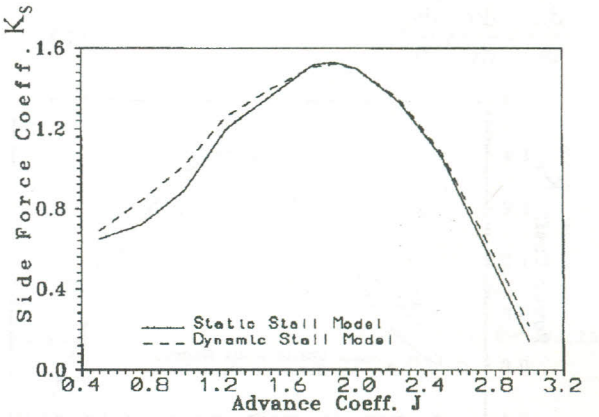

Figure 7 Sculling propulsor side force variation versus advance coefficient with and without dynamic stall [θ=75°]

Two operating conditions are selected to examine the performance more closely; namely J = 0.5 and 1.25. These two conditions were chosen as they fall in the region where dynamic effects are significant. The flow angle to the blade profile at different positions along the blade path is shown in Figure 10-a. At most of the blade path, the stall angle is exceeded.

Due to blade transverse velocity, ship's wake, and induced effects, the local blade section angle of attack, and pitch rate vary periodically with blade position. Maximum incidence is seen to take place at the mid position. The α distribution indicates a variable pitch rate motion. As the

blade is moving inwards, the flow incidence is increasing while it is decreasing when the blade is moving outwards. In other words, $\dot{\alpha}$ is a variable being positive at one side and negative at the other side. Two peak values appear near the extreme edges of the blade path. Equivalent incidence distribution, as calculated from Equations 1 and 2 for both drag and lift is also depicted on the same plot. With such modifications to flow incidence, symmetry in angle of attack distribution no longer exists.

The angle of attack, as well as the modified values for lift and drag for J=1.25 are given in Figure 10-b The blade here is working below stall. The time derivative of angle of attack; $\dot{\alpha}$ is shown in Figure 10-c, where the derivative is calculated as:

$$\frac{d\alpha}{dt} = \frac{d\alpha}{dy} x \frac{dy}{dt} \qquad (13)$$

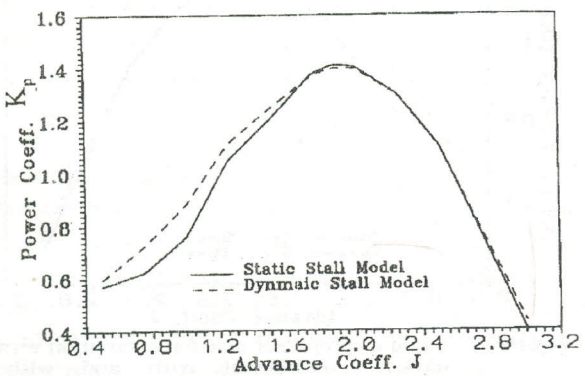

Figure 8 Sculling propulsor power variation versus advance coefficient with and without dynamic Stall [θ=75°]

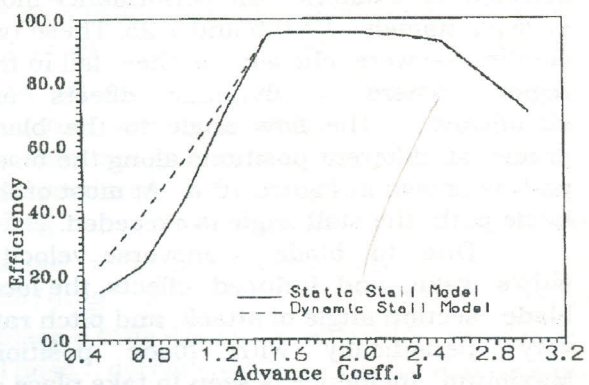

Figure 9 Sculling hydrodynamic efficiency variation versus advance coefficient with and without dynamic stall [θ=75°]

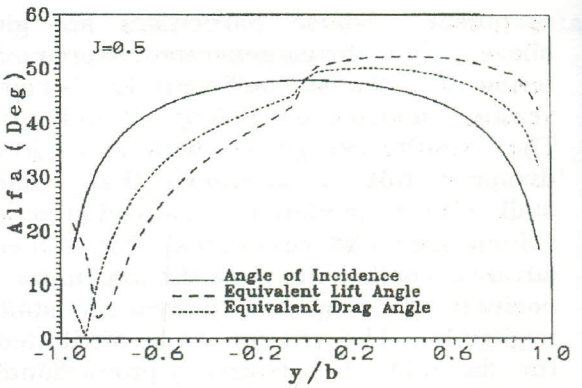

Figure 10-a Angle of incidence and equivalent angles variations along the blade path for J=0.5 and θ=75° sculling propulsor

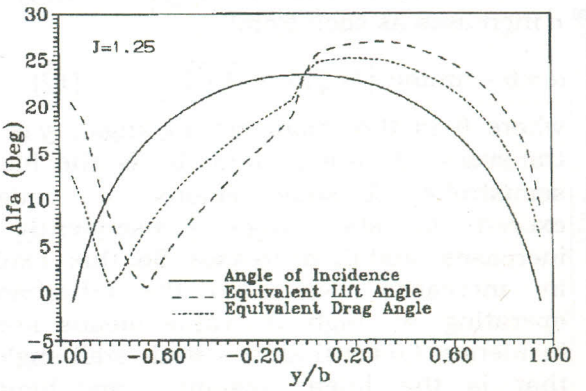

Figure 10-b Angle of incidence and equivalent angles variations along the blade path for J=1.25 and θ=75° sculling propulsor

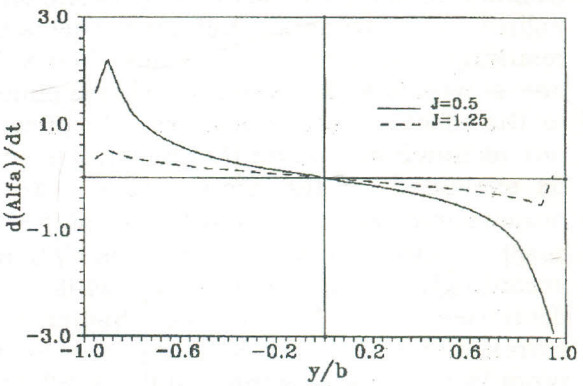

Figure 10-c Pitch rate variations along the blade path for J=1.25 for the θ=75° sculling propulsor

Here, the derivative of y with respect to time is simply the blade transverse speed.

Figure 11-a shows the hysteresis loop in the C_L curve at J = 0.5. The figure indicates two values for lift coefficients at

the same incidence depending on whether the blade is accelerating or decelerating. The figure also depicts the static values for the sake of comparison. At such a low J value, the blade is experiencing incidence values beyond static stall. The motion is characterized by variable pitch rate and different Reynolds numbers. The lift values at J = 1.25 are shown in Figure 11-b together with their static lift distribution. The lift loop is quite narrower at low incidence (below static stall) and gets wider at post stall incidence. The maximum loop width, decreases as the advance speed coefficient increases. Again, this is a variable pitch rate and Reynolds number motion.

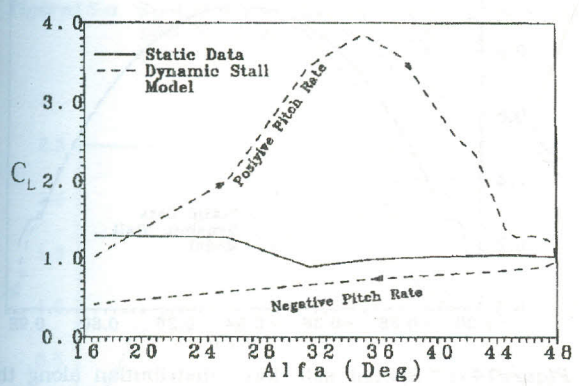

Figure 11-a Lift coefficient hysterisis loop for J=0.5 and θ=75° sculling propulsor

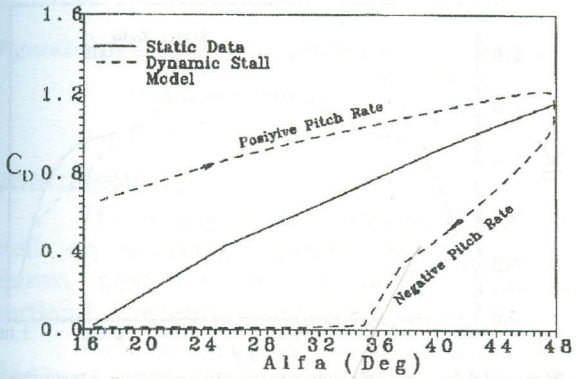

Figure 11-b Drag coefficient hysterisis loop for J=0.5 and θ=75° sculling propulsor

The hysteresis loop in C_D is shown in Figures 12-a and 12-b for J=0.5 and J=1.25 respectively. The drag experienced by the blade, along its transverse motion, and the corresponding incidence is shown. The lower branch displays drag and incidence for the blade while sweeping towards the central plane (pitch is increasing) while the upper leg displays the drag and incidence when the blade is moving outward (pitch is decreasing). At the central plane y/b = 0, the pitch rate is zero and static values are recovered as shown.

The thrust load for the stall calculations shown on Figure 13-a at J=0.5 overshoots to a maximum of approximately 9 times that of the no stall calculations at y/b = -0.8. If maximum loads which occur during the cycle are considered, the stall to no stall value is about 4.

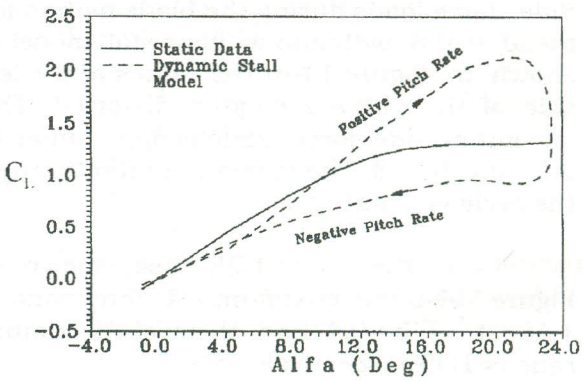

Figure12-a Lift coefficient hysteresis loop for J=1.25 and θ=75° Sculling propulsor

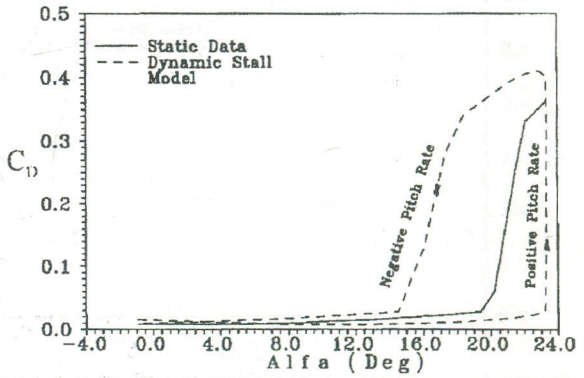

Figure12-b Drag coefficient hysteresis loop for J=0.5 and θ=75° Sculling propulsor

Thrust distribution symmetry about the central plane, in case of using static data, disappears when dynamic stall is considered. Elemental thrust is higher at regions of positive pitch rate and lower at

the side of negative pitch rate. The distribution is characterized by a peak near the port side. The peak thrust magnitude value is 3 times the mean thrust value.

Similar thrust load distribution for another operating condition; namely J=1.25 is shown in Figure 13-b The maximum load in this case, is about 2.7 times of the no stall calculations at y/b = -0.32. Also, the maximum load ratio has dropped down to 0.54. Compared to the J =0.5 case, we may notice that the dynamic stall effect on thrust is less as the advance coefficient gets higher. Again, the thrust distribution along the blade path is not symmetrical. The distribution is characterized by a peak value. The peak location has moved inward. Side force loads during the blade motion for the J = 0.5 with and without stall model is shown in Figure 14-a. The values at the left side of the curve are quite distorted. The maximum side force ratio is approximately 2.2 at y/b= -.8. The maximum ratio through the cycle is about 0.9.

For the J = 1.25 case, shown in Figure 14-b,the maximum side force ratio is 1.68 at y/b=-0.4 and the cycle maximum ratio is 1.39 respectively.

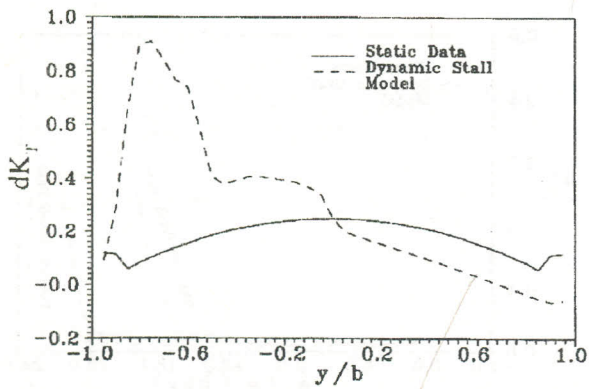

Figure 13-a Spatial thrust distribution along the blade path for J=0.5 and θ=75° sculling propulsor

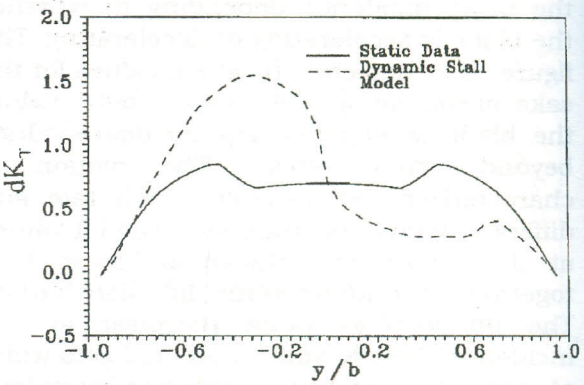

Figure13-b Spatial thrust distribution along the blade path for J=1.25 and θ=75° sculling propulsor

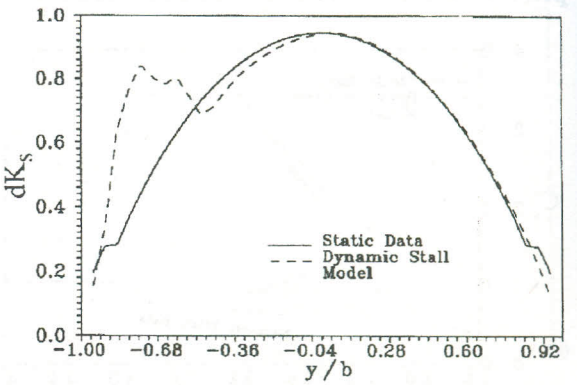

Figure14-a Spatial side force distribution along the blade path for J=0.5 and θ=75° sculling propulsor

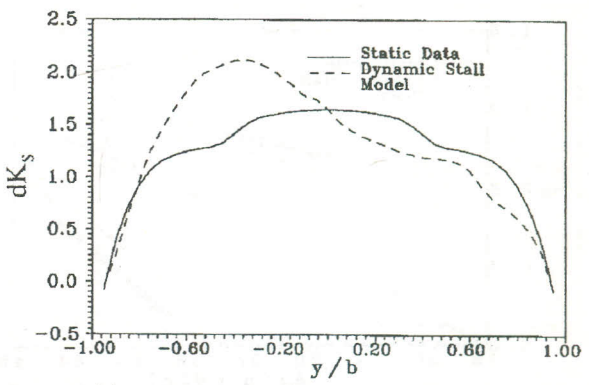

Figure14-b Spatial side force distribution along the blade path for J=1.25 and θ=75° sculling propulsor

Finally, the corresponding input power distributions for the stall and no stall case are shown in Figures 15-a and 15-b for J = 0.5, and 1.25, respectively.

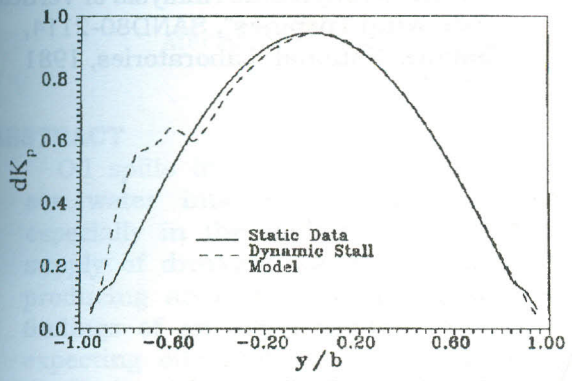

Figure15-a Spatial power distribution along the blade path for J=0.5 and θ=75° sculling propulsor

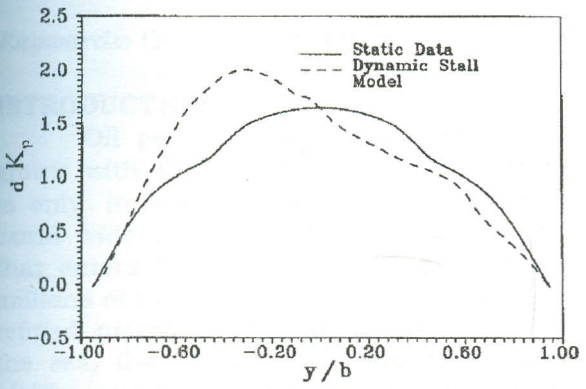

Figure15-b Spatial power distribution along the blade path for J=1.25 and θ=75° sculling propulsor

CONCLUSIONS

The study of the effects of dynamic stall on sculling marine propulsor has shown that stall conditions can occur at partload operating conditions.

The basic result presented for one sculling propulsion system configuration indicates that peak thrust and tangential loads may be significantly underestimated if dynamic stall is not included in the load analysis. The effect of dynamic stall could be more severe since the analysis presented indicates that loads and moments during dynamic stall can be as much as 4 and 9 times the static values, respectively. The consequences of dynamic stall may be a change in performance with resultant mismatch of selected components or reduction in fatigue life of the system structure.

REFERENCES

[1] "Propulsor Efficiency: MIT Penguin Boat Takes Maiden Voyage", Maritime Reporter and Engineering News, May Issue, pp 36, 1997

[2] R, B. Noll, , "Effects of Dynamic Stall on SWECS, Journal of Solar Energy Engineering, Vol.104, pp96-101, 1982

[3] Y. Takamatsu,A. Furukawa, K. Takenouchi, and K. Okuma, " Experimental Considerations in Approximate Method for Estimating the Blade Performance of Darrieus Type Cross Flow Water Turbines", JSME International Journal, Section B., Vol. 36, No. 1, pp.135-142, 1993.

[4] N. D. Ham, and M. S. Garelick, "Dynamic Stall Considerations in Helicopter Rotors"; Journal of American Helicopter Society, Vol. 13, No 2, 1968.

[5] T. Riijarvi B. J. Veitch, and N. Bose, ,"Experimental Performance and Comparison of Performance Prediction Methods for a Trochoidal Propeller Model"; Int. Shipbuilding Progress ,Vol. 41, No. 426, pp113-136. 1994

[6] L.W. Carr, "Progress in Analysis and Prediction of Dynamic Stall": Journal of Aircraft, Vol. 25, No. 1, 1988.

[7] M.R. Visbal, "On Some Physical Aspects of Airfoil Dynamic Stall"; Proceedings of the ASME Symposium on Non-Steady Fluid Dynamics, June 4-7, 1990.

[8] W.J. McCroskey, "The phenomenon of Dynamic Stall", NASA TM- 81264 USA AVRADCOM TR81-A-6.

[9] R. E. Gormont , "A mathematical model of unsteady aerodynamics and radial flow for application to helicopter rotors", USAAMRDL, TR72-67, D210-10492-1, Eustis, Directorates May 1973.

[10] W.Z. Stepniewski, and C.N. Keys, "Rotary Wing Aerodynamics" Dover Publications, Inc., New York, 1984

[11] Kotb, M. A., "Hydrodynamic Performance of Sculling Propulsion System"; Alexandria Engineering Journal, Vol.36, No 6, pp. A281-289, 1997

[12] I.H. Abbott, and A.E. Von Doenhoff, "Theory of Wing Sections",Dover 1959

[13] E. Sheldahl, Robert and Klimas, Paul C., "Aerodynamic Characteristics of Seven Symmetrical Airfoil Sections Through 180-Degree Angle of Attack for use in Aerodynamic Analysis of Vertical Axis Wind Turbines", SAND80-2114, Sandia National Laboratories, 1981